Tectonic activity and earthquake risk in the Chengnanhe fault zone in Weihai city, Shandong province, China, obtained by using an integrated prospecting technique in geophysics and geology

Gui-Lin Du[1,2], Lian-Feng Zhao[3,4,✉], Xiaobo Tian[5,6], Shujuan Su[7], Xiangchun Chang[1], Hualin Wang[8], Zhuqing Huo[9], Tao Zhu[10], and Yonghua Li[10]

[1] *College of Earth Science and Engineering*, *Shandong University of Science and Technology*, *Qingdao* 266590, *China*
[2] *Weihai Earthquake Monitoring Center*, *Weihai* 264200, *China*
[3] *Key Laboratory of Earth and Planetary Physics*, *Institute of Geology and Geophysics*, *Chinese Academy of Sciences*, *Beijing* 100029, *China*
[4] *Mohe Observatory of Geophysics*, *Institute of Geology and Geophysics*, *Chinese Academy of Sciences*, *Beijing* 100029, *China*
[5] *State Key Laboratory of Lithosphere Evolution*, *Institute of Geology and Geophysics*, *Chinese Academy of Sciences*, *Beijing* 100029, *China*
[6] *Innovation Academy for Earth Sciences*, *Chinese Academy of Sciences*, *Beijing* 100029, *China*
[7] *Yantai Earthquake Monitoring Center Station*, *Shandong Earthquake Agency*, *Yantai* 264000, *China*
[8] *Shandong Institute of Earthquake Engineering*, *Jinan* 250014, *China*
[9] *Jiangsu Earthquake Agency*, *Nanjing* 210014, *China*
[10] *Institute of Geophysics*, *China Earthquake Administration*, *Beijing* 100081, *China*

Corresponding author Zhao LF, email: zhaolf@mail.iggcas.ac.cn

Key points:

- A case study to detect tectonic activity and to estimate earthquake risk by using the integrated geophysical and geological techniques.
- Images for seismic reflection profile, electrical resistivity, geologic section of boreholes, and exploration trench are obtained for the Chengnanhe fault.
- Both the geophysical and geological results reveal that the Chengnanhe fault is relatively stable and inactive.

Abstract For city planning and reducing potential earthquake risk, it's necessary to detect the information of the buried faults in an urban area especially, including the location and activities. An integrated technique with geophysical and geological methods, including the shallow seismic reflection profile, electrical resistivity measurement, geologic borehole section, and exploration trench, was used to detect the Chengnanhe fault, which is one of the two main faults passing through the Weihai urban area in Shandong province, China. The results show that it is a normal fault striking with E-W direction, and it is relatively inactive and stable. By using the thermoluminescence (TL) dating, we found that the Chengnanhe fault initiated in mid-Pleistocene and there was no offset after late Pleistocene. Such an integrated technique with multiple geological and geophysical methods provides a significant assessment of earthquake risk for city planning in urban areas.

Keywords: Chengnanhe fault; geologic drilling; thermoluminescence (TL) dating; shallow seismic profile; electrical resistivity measurement

Citation: Du GL, Zhao LF, Tian XB, Su SJ, Chang XC, Wang HL, Huo ZQ, Zhu T, and Li YH (2021). Tectonic activity and earthquake risk in the Chengnanhe fault zone in Weihai city, Shandong province, China, obtained by using an integrated prospecting technique in geophysics and geology. Earthq Sci **34**, doi: 10.29382/eqs-2020-0058

Received 3 March 2021.

1 Introduction

It is important for city planning to detect the subsurface fault in an urban area; and the integrated methods in geophysics and geology have been proven to be the most effective in investigating urban faults (Deng QD, 2002). To explore shallow structure, several geophysical methods can be used for general survey, such as seismic reflection profile, electromagnetic sounding, microgravity, and so on (Arjwech et al., 2020; Wang ZC et al., 2006; Wang ZH et al., 2018). Based on the results from general survey, some regions will be determined as the detailed investigation areas. The geology methods, such as the trench excavation and joint section of drilling, can be adopted sequentially for fine structures in these areas (Guo H et al., 2011; Ran YK et al., 2014; Xu XW et al., 2009). By using the integrated methods in geophysics and geology, active faults can be explored in details, including their locations and activities (Deng QD, 2002; Liang K et al., 2018).

Figure 1 shows our study area in Weihai city, Shandong province, China. The Weihai city is situated in a mountainous area in the east of Jiaodong peninsula. The thick sediments cover the Quaternary basin between the mountains. As two main faults, the Chengnanhe and Shendaokou faults pass through the Weihai urban areas, as shown in Figure 2. Several sensible earthquakes occurred in Weihai urban areas in recent years, such as Rushan earthquake swarm (Zheng JC et al., 2017). From a regional perspective, the Weihai city is affected by the Tanlu fault and the Penglai-Weihai fault zones. The impact intensity of the 1668 Tancheng earthquake (M_S8.5) reached to 7 degrees in Weihai city. Compared with the Tanlu fault zone, the Penglai-Weihai fault zone has a more direct impact on this region (Wang ZC et al., 2006). As a significant fault zone in the Shandong peninsula, the Penglai-Weihai fault zone affects the level of seismic activities in Yantai and Weihai cities (Wang ZC et al., 2006). The 1548 Bohai *M*7 earthquake and the 1948 northwest sea of Weihai *M*6 earthquake occurred in the

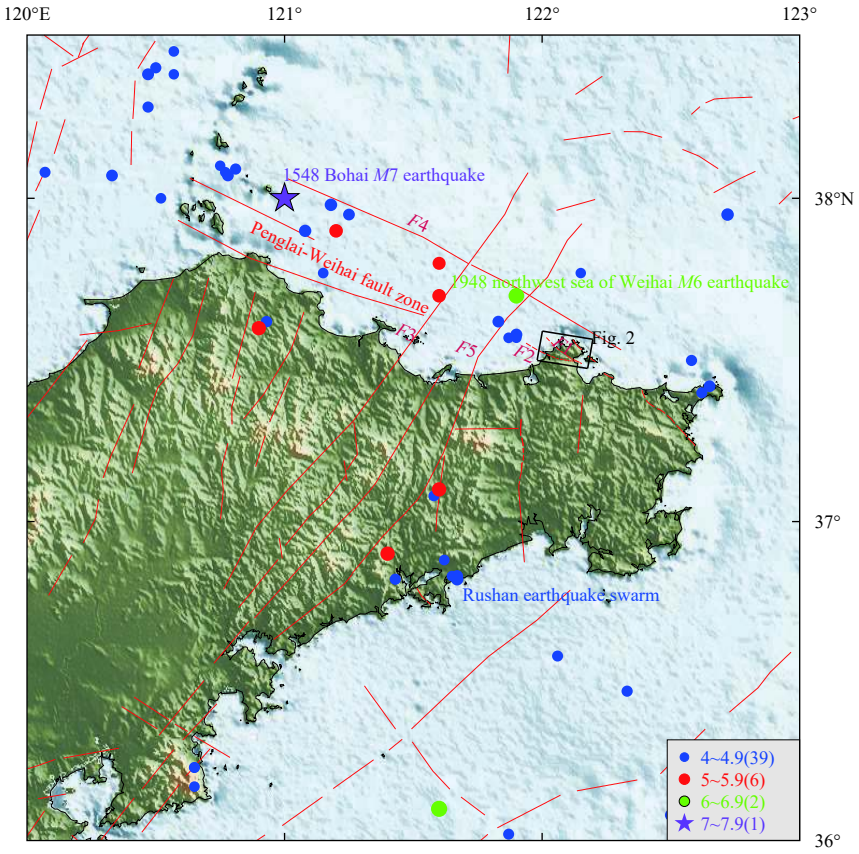

Figure 1 Structural sketch of the Penglai-Weihai fault zone. The pentagrams are the locations of the 1548 Bohai earthquake with magnitude larger than 7 (8>*M*≥7). The green circles represent the locations of with magnitude 6 (7>*M*≥6), and the northwest sea of Weihai *M*6 earthquake are marked in the figure. The red circle represents the locations of event with magnitude 5 (6>*M*≥5), and the blue circles represent the earthquake locations of magnitude 4 (5>*M*≥4). The red lines represent the locations of faults and the black box indicates the study area. The abbreviation: *F*1, Shendaokou fault; *F*2, Chengnanhe fault; *F*3, Taocun-Dongdoushan fault; Dazhudao-Weihaibei fault (*F*4), Haiyang fault (*F*5)

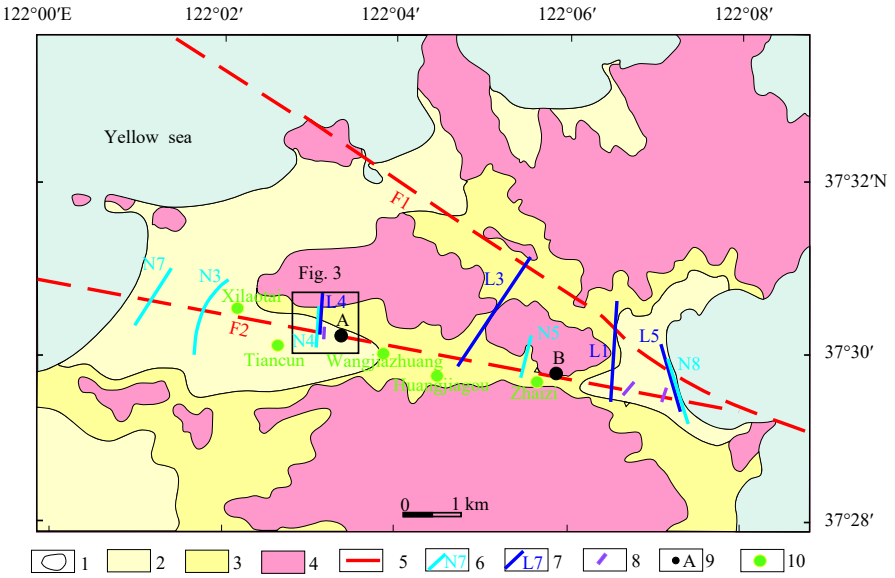

Figure 2 Maps showing tectonics in the Weihai urban area, with legends including 1: Boundary of geological blocks, 2: Holocene, 3: Upper Pleistocene, 4: Lower Proterozoic – Archean Diorite, 5: Shendaokou fault (*F*1) and Chengnanhe fault (*F*2), 6: High-density electrical method detection profile and serial number, 7: Shallow seismic profile and serial number, 8: Geologic section of boreholes and serial number, 9: Exploration trench and serial number, and 10: The location of villages.

western and eastern segments of the Penglai-Weihai fault zone respectively (Figure 1). Furthermore, in Weihai city areas, the Chengnanhe fault is regarded as a southern boundary fault of the east of Penglai-Weihai fault zone (Figures 1 and 2). The previous studies on this fault lack the fine structures so as not to satisfy the earthquake safety assessment and growing urban planning (Wang HL, 1998). Therefore, it would play an extremely important role in studying the activity of the Chengnanhe fault for urban construction as well as land exploitation and utilization in Weihai urban areas.

2 Methods

This study aimed to detect the location and activities of Chengnanhe fault in Weihai urban areas by means of integrated geophysical and geological methods (Arjwech et al., 2020; Ma ZX et al., 2018; Suski et al., 2010; Xu XW et al., 2016; Zhu JF et al., 2005). Firstly, the location of the fault was detected by seismic reflection and electrical resistivity imaging. Secondly, the location and the active age of Chengnanhe fault was accurately detected by means of joint drilling section. Thirdly, the latest active age of the fault was ascertained through stratigraphic and chronological test analysis of trench excavation. Finally, fault- crossing leveling survey was a useful method to get the relative movement on both sides of the normal fault.

2.1 Geophysical methods

The shallow seismic exploration and high density electrical exploration were used in investigating the Chengnanhe fault. The field data collection was completed for shallow seismic exploration in August 2006. High density electric exploration was completed in September 2006. Seismic reflection wave method can effectively detect the buried depth and velocity structure of stratum or rock mass so as to identify faults. It has been widely and effectively applied in active fault detection (Feng SY et al., 2010; He ZQ et al., 2007; Liu BJ et al., 2002). In the field construction of shallow seismic reflection detection, the survey line should be as vertical as possible to the fault strike, span and effectively control the fault, and be far away from the site environment of various disturbance sources (Hu G et al., 2016; Ma ZX et al., 2018). To reduce the impact of urban interference on seismic detection and improve the signal-to-noise ratio, an electric drop hammer (ESS-200) with 1500 kg weight was used in this shallow seismic exploration. The seismometers used three combinations of JF-SD-60 Hz geophone placed on the iron block, and the SUMMIT high-resolution digital seismograph from Germany was used for data collection. Data processing software WinSeis package we used was from Kansas Company, USA. The final high-resolution seismic reflection time profile for geological interpretation was obtained from a series of single shot data collected in the field and processed with certain procedures.

Seismic reflection wave method usually adopts common reflection point multiple coverage observation system. The time-distance curve equation of the reflected wave in the superimposed trace set of common depth points can be written in the following form (Lu MJ, 2001),

$$t_k = \frac{1}{V} \cdot \sqrt{4H^2 + X_k^2}, \quad (1)$$

where X_k is the shot interval, H is the depth of the interface and V is the interval velocity. If X_k equals 0, t_0 equals $2H/V$ and is the travel time of normal line at common midpoint. From the time-distance curve equation of the reflected wave at the common shot point, the normal time difference of the reflected wave curve equation at the common shot point can be obtained as follows (Lu MJ, 2001),

$$\Delta t_k = t_k - t_0 = \sqrt{\left(\frac{X_k}{V}\right)^2 + t_0^2} - t_0. \quad (2)$$

During the data processing, the time-distance curve of the common reflection point of the hyperbolic line is corrected to a straight line after normal moveout correction. After repeated superposition, the reflection signal equivalent to self-excited and self-received signal at the point M with enhanced energy can be obtained. After the data of multiple measuring points on the measuring line are processed by the above method, a set of superposition time profile reflecting the self-excited and self-received information at each point can be obtained. This method has obvious effect on suppressing interference wave and improving signal-to-noise ratio. By analyzing and comparing the wave formation characteristics of time section and combining with geological data, the structural morphology and stratigraphic properties of each reflected layer can be determined, and then the strike, dip and location of possible faults can be determined (He ZQ et al., 2007; Hu G et al., 2016).

Compared with seismic methods, electrical resistivity imaging has some advantages especially in its limited sensitivity to urban noise, and has an effective depth investigation of several hundred meters, so that this technique has been one of the most powerful geophysical tools for detecting a buried fault in an urban area (Suski et al., 2010; Zhu T et al., 2017). The electrical resistivity measurement equipment used in this study was the MIR-2000 resistivity meter. The instrument belongs to a centralized measurement system, each array can control the number of electrodes at most 120, with a variety of measurement, data automatic acquisition and real-time processing functions. As the target area of this detection is in the urban area of Weihai City, and the observation environment is relatively complex, which requires easy to set up the survey line, strong anti-interference ability of the observation device, so that we use the electrical prospecting based on Winner arrangement.

When using the high-density electrical method, electrodes A and B are used for providing electric power to electrodes M and N. The instrument directly measures the potential difference which is shortened as U_{MN} (The unit is mV) and the supply current which is shortened as I (The unit of I is mA) between electrodes M and N. The midpoint of M and N electrodes was taken as the data recording point, and the formula of its apparent resistivity ρ_s was (Shen HY, 2012; Zhu T et al., 2009),

$$\rho_s = \frac{U_{MN}}{I} \cdot K, \quad (3)$$

where K is the geometric factor with respect to electrode spacing and can be expressed as,

$$K = \frac{2\pi}{\left(\frac{1}{AM} - \frac{1}{BM}\right) - \left(\frac{1}{AN} - \frac{1}{BN}\right)}. \quad (4)$$

Among them, the Wenner and pole-pole arrays have maximum intensity coefficient, thus they have the strongest anti-disturbance ability (Shen HY, 2012; Zhu T et al., 2009). Data processing software RTS-1 package that we used is from the Institute of Geophysics, China Earthquake Administration (Hao JQ et al., 2000; 2002). The electrical discontinuity in the resistivity image becomes an important symbol for tracing the fault.

2.2 Geological methods

Through borehole joint section and trench excavation, combined with stratigraphic and chronologic test analysis, the latest active age of the fault can be determined (Ran YK et al., 2014). On the basis of geophysical explorations, geological borehole joint profile is an important means to detect buried faults. It has been well applied in the detection of the Tangshan, Xiadian and Yinchuan faults (Guo H et al., 2011; Hu P et al., 2010; Liu BJ et al., 2008). In geological drilling exploration, it is necessary to establish a standard formation borehole with well-developed Quaternary system. It is also important to determine in detail the age of each Quaternary formation in the standard borehole so as to provide a basis for the stratigraphic correlation of the joint borehole section in the later geological drilling. The initial boreholes need to have a little more distance across the fault, and then depending on the actual situation, more holes are drilled until the fault is located. By comparing the characteristics of formation behavior and thickness variation in boreholes on both sides of the joint borehole section, we can find the relative difference between the fluctuation movement of the han-

ging wall and footwall of the fault. Finally, the latest active age of the fault is determined by the age of the offset strata and the overlying strata. In August 2007, based on shallow seismic exploration and high-density electrical exploration, we chose to lay a joint borehole section near Fushan Road with the most obvious characteristics of the break point to detect the activity of Chengnanhe Fault.

Trench excavation is the most direct way to study the fault if the overburden is not very thick (Ran YK et al., 2014). Trench excavation is one of the most effective methods to study seismogenic structures and has been widely used in large earthquakes such as Wenchuan earthquake and Tangshan earthquake (Guo H et al., 2011; Xu XW et al., 2009; Xu XW et al., 2010). We can directly study the fault activity age and activity properties through the trench profile. In October 2012, through the foundation pit excavation at the construction site on the east side of Weihai No.9 Middle School near Fushan Road, the Chengnanhe Fault was clearly shown to us. In this study, we determined the occurrence and activity age for the Chengnanhe fault.

2.3 Fault- crossing leveling survey

The fault-crossing leveling survey, showing great variations before some large earthquakes, is an important seismic monitoring method. For example, the east-west transverse fault level in Jinxian County fluctuated before the 1975 Haicheng *M*7.3 earthquake (Wang KL et al., 2006). The fault-crossing leveling has been used to analyze recent activities of the faults in other places (Saberi et al., 2017).

The fault-crossing leveling observation of the Chengnanhe fault is located within the playground of Weihai No. 9 Middle School (Figure 3). The total length of the survey line is 160 meters. The starting point is named *A* and the end point is named *B*, point *A* and point *B* are all located on the bedrocks. Between point *A* and point *B*, there are three transition points (G1, G2, and G3) in the middle (Figure 3). The observation instrument, produced by Trimble Company in the United States, is DINI03 digital level. This instrument is one of the most accurate digital level (DS1 level) at present. The observation of cross-fault leveling site in Weihai No. 9 Middle School was initiated from July 2016.

3 Results

3.1 Basements of the rocks reveled by shallow seismic exploration

In the shallow seismic exploration, four reflection lines

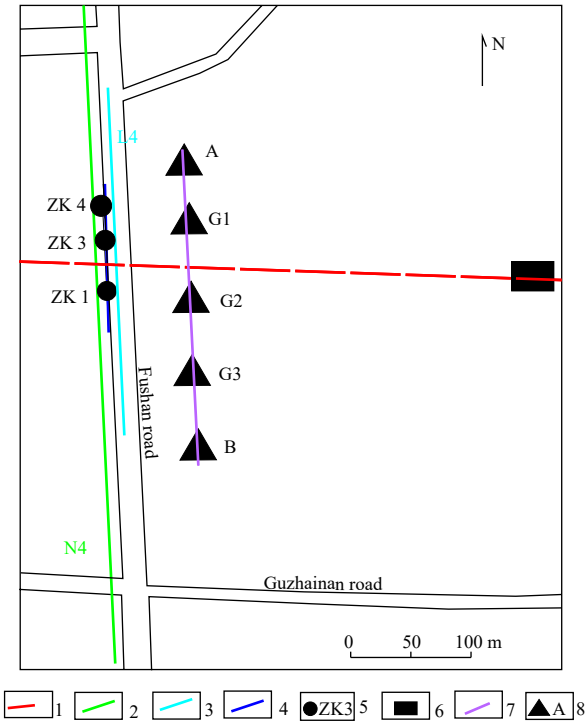

Figure 3 Sketch map of the survey lines, with legends of 1: Chengnanhe fault, 2: electrical resistivity imaging profile (N4), 3: shallow seismic profile, 4: geologic section of boreholes, 5: drill hole and serial number, 6: exploration trench, 7: the line of fault-crossing leveling at Weihai No. 9 Middle School, and 8: the observation point on the line of fault-crossing leveling and serial number.

(L1, L3, L4 and L5) were laid out for Chengnanhe fault (Figure 2), and four breakpoints were obtained. The typical breakpoints of Chengnanhe fault obtained by shallow seismic exploration were briefly introduced at ordinate origin of line L4, the cophasal axes on seismic section were staggered, namely, the north plate relatively slip down for about 8 ms (about 5 m).The fault with fault plane inclining to the north at a high angle was a normal fault. The buried depth of the upper breakpoint was less than 12 m (two-way travel time was about 18 ms), near the breakpoint, emission wave was significantly weakened, which may be caused by the Chengnanhe fault (Figure 4).

3.2 High-density electrical profiles

In this study, five high-density electrical detection lines (N3, N4, N5, N7 and N8) were deployed for the exploration of the Chengnanhe fault, and 5 electrical discontinuities were obtained (Figure 2). The typical electrical discontinuities obtained from line N4 of the west side of the Fushan road were briefly introduced in this paragraph. The line N4 was located in the west side of the Fushan road, revealing that the thickness of cover layers in detection area was about 16 m. Bounded by a horizontal

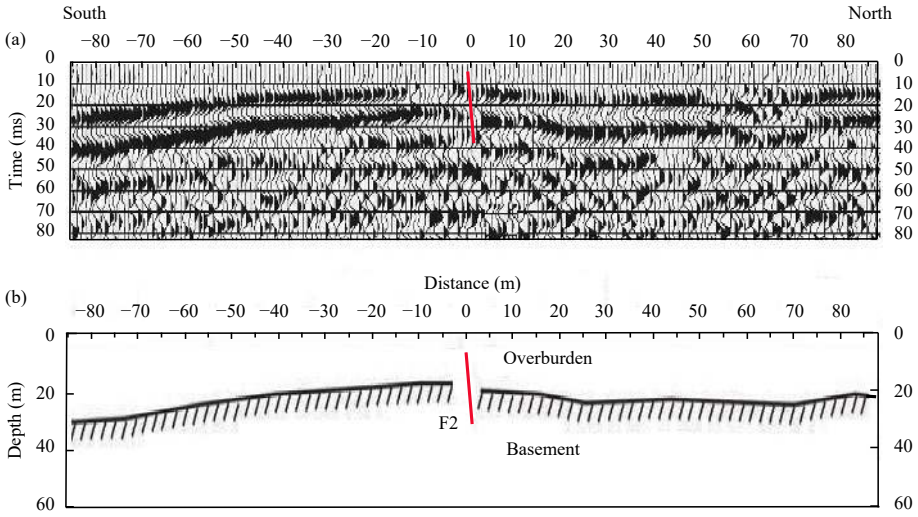

Figure 4 Shallow seismic profile across the Chengnanhe fault (red lines) (a) and interpreted depth section (b)

coordinate of ordinate origin, the bedrock was divided into the southern area and the northern area with obvious electrical differences. The electrical structure of southern area was relatively messy, showing a lower resistivity value, meanwhile, the electrical structure of northern area was very complete, showing a higher resistivity value. It can be inferred that the apparent dip angle of the fault plane is about 79°, with a southward dip direction, and the buried depth of the upper breakpoint was about 16 m. The abnormal structure of electrical property showed V-shaped (Figure 5).

3.3 Images of joint geological drilling exploration

In the working of seismic zoning in Weihai city, the Quaternary stratigraphic standard section of Weihai city was established by detailed stratigraphic catalogs and TL dating of samples, which provides a basis for determining the active age of faults (Wang HL, 1998). Based on the results of shallow seismic expleration and high-density electrical detection method, the geologic section DP1 with 3 boreholes was laid out in the presumed Chengnanhe fault (west of the Fushan road). The boreholes numbers are ZK1, ZK3 and ZK4, respectively. The distance between boreholes ZK3 and ZK4 was about 43 m, and the distance between boreholes ZK1 and ZK3 was about 64 m (Figure 6).

The borehole shows that Quaternary cover layers, with a thickness of 6.3–8.4 m, underlying bedrock beneath the cover layers being granite gneiss, can be divided into 6 layers from the top to the bottom. Firstly, 1.2–2.3 m thick can be revealed for the first layer with the miscellaneous filling soil, brownish red to yellowish brown, mainly silty clay, containing stones, coarse sand. To the second layer, the silt clay, gray black, soft plastic-plastic, with high sand content in the upper part and high clay content in the middle and lower part, add up to 1.4–2.8 m thick. The TL dating age of the second Layer was 52.4 ± 2.6 ka (Figure 6). The third layer revealed in the drilling is the 7.6 m thick silt clay with iron-manganese nodules, brown yellow to reddish brown, plastic, medium dense, containing iron-manganese nodules and coarse sand particles, locally contained gravel, particle size of 2–5 cm, sand-soil

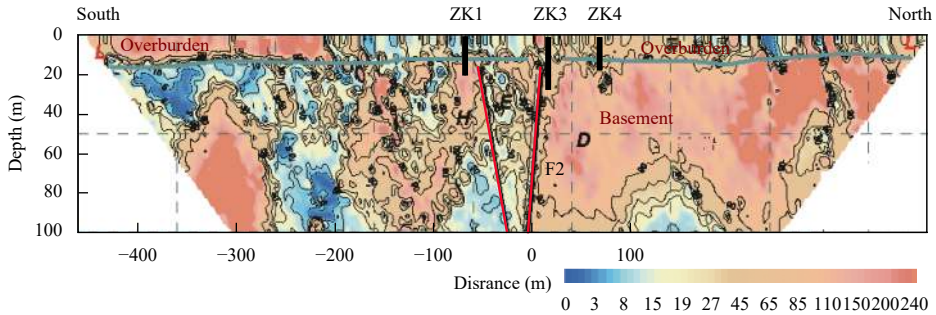

Figure 5 Electrical resistivity imaging profile of the Chengnanhe fault. The thickness of the overburden sediments is about 20 m. The sediments have relatively low resistivity, whereas the basement is characterized by high resistivity. The F2 represents the Chengnanhe Fault.

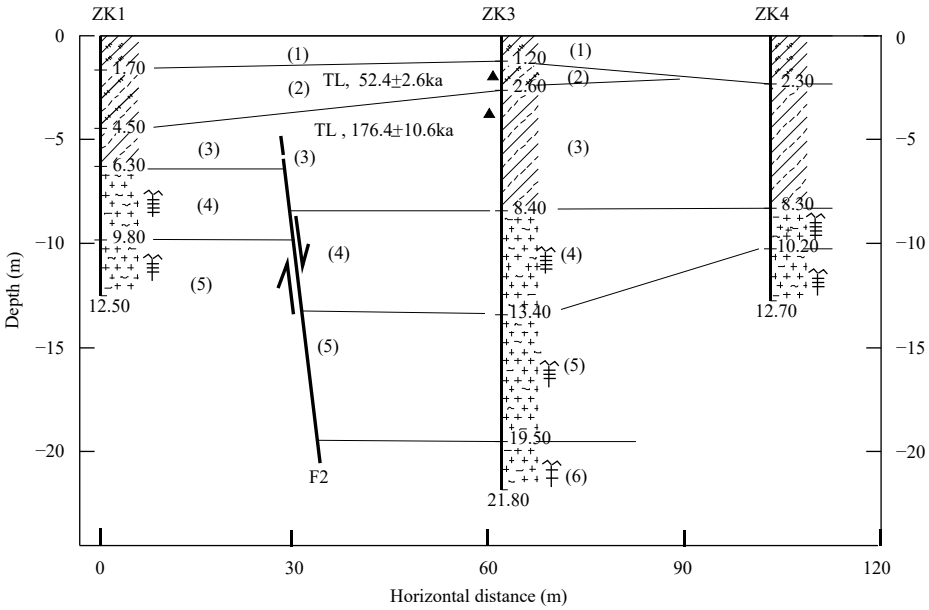

Figure 6 The geologic section of boreholes from ZK1, ZK3 to Zk4, where six layers can be determined by (1) the Miscellaneous fill, (2) silt clay (The black triangle denotes TL sampling point), (3) silt soil, (4) fully weathered granite gneiss, (5) strong weathered granite gneiss, and (6) moderately weathered granite gneiss, respectively.

core. The TL dating age of the third layer was 176.4 ± 10.6 ka (Figure 6). The basement revealed by the boreholes that was located beneath the third layer and was divided into three layers. The fourth, fifth and sixth layer were fully weathered granite gneiss, strongly weathered granite gneiss and moderately weathered granite gneiss respectively. The fourth layer has a feature of gray-black, original rock texture, completely destroyed structure, core with sand-column shaped, and the thick is 1.9–5.8 m. The fifth layer is composed of strong weathered granite gneiss with gray-black, coarse-grained, primary texture, massive structure, core of sand column, and the thick is 3.5–6.1 m. The sixth layer has massive structure, core of massive and short-column that was concealed beneath the soil, with a maximum exposed thickness of 2.3 m.

Through the geologic section, it was speculated that the fault roughly located between boreholes ZK1 and ZK3. There was a drop of 2.1 m on the bottom boundary of the Mesozoic Pleistocene silty clay on both sides of the faults and a drop of 7.0 m on the bottom boundary of strongly weathered granite gneiss, indicating the movement characteristics of the Chengnanhe fault fell in the north and raise in the south. It was proved that the horizontal location and dip direction of Chengnanhe fault obtained from seismic reflection and electrical resistivity imaging were correct. From the TL dating age of the second layer and the third layer, the two layers belong to Middle Pleistocene. The fault does not offset the two overlying layers, so that we speculate that Chengnanhe fault was not active since the late Pleistocene epoch.

3.4 Trench excavation section

The Chengnanhe fault was exposed to the east side wall of foundation excavation at a construction site, which lied in the east side of the Weihai No.9 Middle School. The excavation point was about 300 m from east of the Fushan road. The strongly broken fracture zone mainly composed by crushed-silt rock had a width of 4 m. The fault gouge was not observed. The bedrock on both sides against the fault was relatively complete. The upper part of the main fault surface, a thickness of about 4 m, was covered with the Quaternary residual slope deposit. The lower part of the residual slope deposit showed a nearly horizontal sedimentary bedding, showing the fault's inactivity since the late Pleistocene. According to the dating analysis of the laboratory in the Shandong Institute of Earthquake Engineering, the TL dating age of the overlying strata was 48.9 ± 1.7 ka (Figure 7). It means that the Chengnanhe fault that belongs to a Middle Pleistocene fault has been inactive since the late Pleistocene.

3.5 Monthly-average elevation changes

The monthly-average elevation changes of fault-crossing leveling in Weihai No. 9 Middle School show a good annual variation characteristic, with a downward trend in the first half year and an upward trend in the second half year from July 2016 to December 2020. At present, it is in the ascending stage with normal annual variation characteristics (Figure 9). This annual variation is mainly affected by rainfall. This can also prove that the

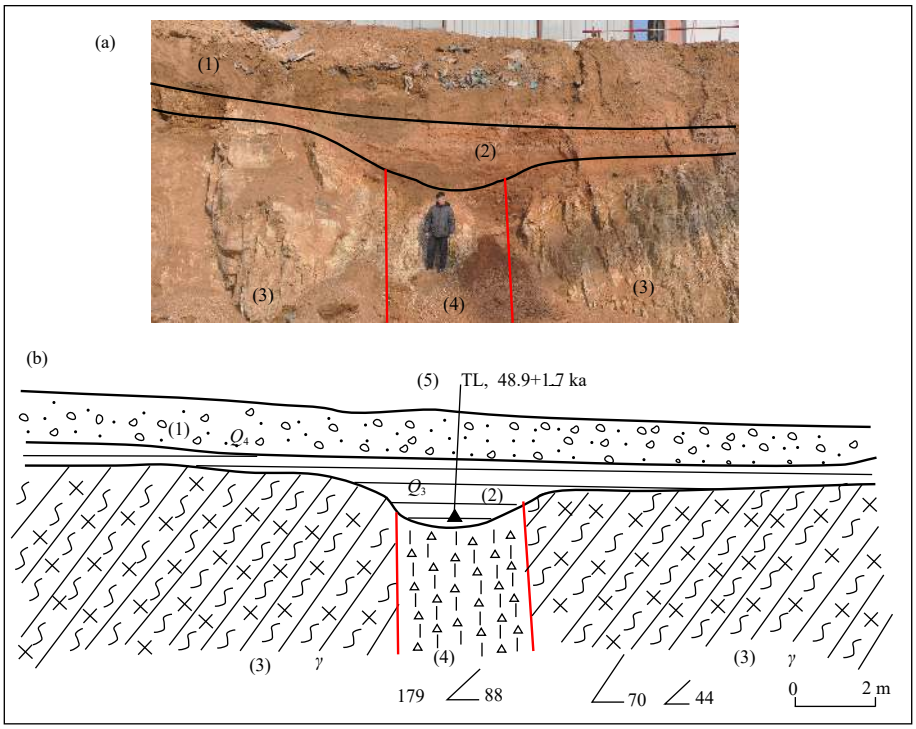

Figure 7 Map showing the exploration trench with a photograph (a) and a geological interpretation section of the Chengnanhe fault (b), where (1) is the residual slope deposit, (2) the Late Pleistocene sandy soil, (3) granite gneiss, (4) Fault and (5) the TL sampling point.

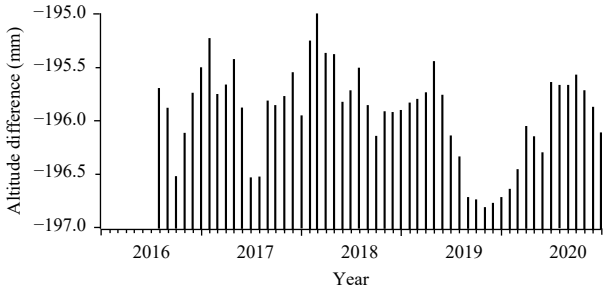

Figure 8 Map showing the altitude difference data of fault-crossing leveling in Weihai No. 9 Middle School.

Chengnanhe fault has been relatively inactive from the other aspect. However, this stability of the Chengnanhe was obtained based on relatively short time observations. Therefore, it is necessary to evaluate the movement characteristics of the fault through long-term observations.

4 Discussions

The Penglai-Weihai fault zone can be divided into two segments by the Taocun-Dongdoushan fault (Wang ZC et al., 2006). The western Changdao-Yantai segment is a late Pleistocene active segment, where the 1548 Bohai *M*7 earthquake occurred (Figure 1). The eastern Yantai-Weihai segment is a mid Pleistocene segment on which no late Pleistocene offset has been found and no magnitude more than *M*7 earthquake occurred. Compared with the west segment, the east one is relatively inactive. On the other hand, the intersection regions of the Penglai-Weihai fault zone with NE striking fault zones are considered to be the likely places for the future medium to strong earthquakes (Wang ZC et al., 2006). This is the main reason why the 1948 Weihai *M*6 earthquake occurred on the intersection of the Dazhudao-Weihaibei fault (F4) and NE striking Haiyang fault (F5). In other word, it is likely that no late Pleistocene fault such as Chengnanhe fault don't insect with NE striking fault would not occur medium to strong earthquakes.

In this study, we determined the exact locations where the Chengnanhe fault passes through the Weihai city. The Chengnanhe fault starts from the south of Weihai urban area, roughly along the Chengnanhe river, through Zhaizi village, Huangjiagou village, Wangjiazhuang village, to the south of Xilaotai village and Yandun hill, and finally extends into the sea (Figure 2). The overall trend of the Chengnanhe fault is about 280° and the length of the land part is about 9.7 km. In terms of topography and geomorphology, apart from coastal areas of the south of the city in the eastern part of the Chengnanhe fault, there are mostly low hills and Piedmont slope areas in the south, while in the north, a slightly decrease can be seen, so the thickness of the Quaternary cover layers has been slightly

increased. From the south of the Naigu hill to the west to Tiancun village, the fault is characterized by a wide valley landform which is slightly open to the west. The west segment of the fault, located in the west of Tiancun village, is concealed beneath the Quaternary plain.

In the process of geophysical exploration near Fushan road, it was found that the fault occurrence form shallow seismic exploration and resistivity imaging is inconsistent. In shallow seismic exploration, the fault sloped to the north while the resistivity imaging shows a V-shaped property, which is caused by the uncertainty of geophysical exploration methods. However, the location of the fault determined by geophysical exploration results was quite consistent, especially the results of shallow seismic exploration and resistivity imaging fault morphology were close to the results of borehole joint profile. The scattering around the fault on the south side of shallow seismic exploration was more obvious, while that on the north side was relatively consistent. On the resistivity image, the southern side of the fault was cluttered while the northern side of the fault footwall is intact. Both the joint geological drilling exploration and the trench excavation can detect the location and the dating of the fault, but the trench excavation can reveal the fault to us more clearly. The trench excavation is the most direct fault detection method, but not all places is suitable for excavation, because of its expensive cost.

5 Conclusions

After the active fault survey, reasonable measures should be taken to avoid seismic hazard caused by active fault for general land-use planning and building construction (Xu XW et al., 2016). This preventive measure is significantly important to improve our capability of earthquake disaster reduction (Deng QD et al., 2007). The Chengnanhe fault has no obvious indication in topography and landform, only bedrock scarps and slopes are found locally. According to the results of shallow seismic exploration and high-density electrical detection, the location of the fault was found out. Combined with the analysis of drilling joint geological section and trench, the Chengnanhe fault with a width of 3 to 7 m, that belong to a Middle Pleistocene fault, has been inactive since the late Pleistocene.

The seismic risk of the Chengnanhe fault is generally evaluated by using the tectonic analogy method. In eastern China, the largest earthquake magnitudes associated with the Middle Pleistocene fault range from 5 to 6 (Xiang HF et al., 2008). Specifically in Shandong Province, it is suggested that the maximum earthquake magnitudes induced by the Middle Pleistocene fault may be 5.5 (Wang ZC and Chao HT, 1999). As a buried inactive normal fault of the Middle Pleistocene, the influence of the seismic fault dislocations near surface can be neglected, just like those observations from active fault survey in the Lanzhou city (Yuan DY et al., 2008). However, the impacts of unevenness need to be considered in foundation treatment during the building construction (Wang HL, 1998). The results in this study provided a significant basis for the urban planning and seismic design of the urban construction in Weihai city.

To detect the society of an active fault and assess the earthquake risk for Weihai city, we tested a series of detection methods in geophysics and geology in this study. First of all, based on the uncertainties in geophysical exploration, two or more geophysical methods were combined to detect the approximate location and scale of the active faults, and provided a preliminary result for the city planning and site selection in a new urban area. For instance, the shallow seismic exploration and high density electrical method can be used for this purpose. Based on this consideration, the kinematic characteristics and activity date of faults can be determined by joint geological drilling exploration and accurate dating analysis technique. Finally, by using the technology of trench excavation, we can obtain the latest active age of faults and then provide some conclusions for the planning and site selection of new urban areas. The detection flow used in this research can be a helpful reference to investigate the active fault in other cities.

Acknowledgments

This work was supported by the Special Fund of China Seismic Experimental Site (Nos. 2019CSES0103, 2018CESE0102 and 2016CESE0203), the National Natural Science Foundation of China (Nos. 41630210, 41674060, 41974054, and 41974061), and the “Active Faults Exploration and Seismic Hazard Assessment in Weihai City” funded by Weihai Municipal People's Government. Some figures were made using Generic Mapping Tools (https://forum.generic-mapping-tools.org/, last accessed March 2020)(Wessel et al., 2013)

References

Arjwech R, Boonsungnern W, Sriwangpon P, Somchat K, and Pondthai P (2020). Using integrated geophysics data set to delineate Phetchabun active fault in Thailand. Data in Brief **30**:

105608.

Deng QD (2002). Exploration and seismic hazard assessment of active faults in urban areas. Seismol and Geol **24**: 601–605 (in Chinese with English abstract).

Deng QD, Lu ZX, and Yang ZE (2007). Remarks on urban active faults exploration and associated activity assessment. Seismol Geol **29**(2): 189–200 (in Chinese with English abstract).

Feng SY, Long CX, Gao R, Shi JH, Yang ZX, Tan YL, and Kou KP (2010). Joint application of high-resolution refraction and shallow reflection seismic exploration approach to active fault survey. Acta Seismologica Sinica **32**(6): 718–724 (in Chinese with English abstract).

Guo H, Jiang WL, and Xie XS (2011). Late-Quaternary strong earthquakes on the seismogenic fault of the 1976 M_S7.8 Tangshan earthquake, Hebei, as revealed by drilling and trenching. Sci China: Earth Sci **54**(11): 1 696–1 715.

Hao JQ, Feng R, Zhou JG, Qian SQ, and Gao JT (2000). Resistivity tomography study on samples with water-bearing structure. Acta Seismologica Sinica **13**(3): 325–330.

Hao JQ, Feng R, Zhou JG, Qian SQ, and Gao JT (2002). Study on the mechanism of resistivity changes during rock cracking. Chin J Geophys **45**(3): 440–449 (in Chinese with English abstract).

He ZQ, Chen YK, Ye TL, Wang XD, Wang H, and Jia H (2007). Application of shallow seismic exploration in detecion of buried fault in coastal areas. Seismol Geol **29**(2): 363–372 (in Chinese with English abstract).

Hu G, He ZQ, Li N, and Ye TL (2016). Detection of the northern section of Anninghe fault zone by seismic reflection method. Acta Seismologica Sinica **38**(6): 813–823 (in Chinese with English abstract).

Hu P, Liu BJ, Bai LX, Mu HW, Zhang J, Ding YH, Luo HC, and Feng R (2010). Synthetic exploration of the buried faults in Olympic park area. Chin J Geophys **53**(6): 1 486–1494 (in Chinese with English abstract).

Liang K, Sun CB, Ma BQ, Tian QJ, Li DW, Li DW, and He ZT (2018). Investigation of the Yellow River buried fault in the Wuhai basin, northwestern Ordos Block, China, using deep/shallow seismic reflection and drilling techniques. J Asian Earth Sci **163**: 54–69.

Liu BJ, Chai CZ, Feng SY, Zhao CB, and Yuan HK (2008). Seismic exploration method for buried fault and its up-breakpoint in Quaternary sediment area-An example of Yinchuan buried active fault. Chin J Geophys **51**(5): 1 474–1483 (in Chinese with English abstract).

Liu BJ, Zhang XK, Fang SM, Zhao CB, Duan YH, Zhu JF, Huang Z, Huang ZL, Wang SX, and Zheng DG (2002). Acquition technique of high-resolution shallow seismic data for surveying of urban active faults. Seismol Geol **24**(4): 524–532 (in Chinese with English abstract).

Lu MJ (2001) Principles of Seismic Exploration. The third edition. Dongying, Petroleum University Press, .

Ma ZX, Zhang GH, Chen XG, Zhao GC, Ding R, and Li GC (2018). Shallow structural characteristics and spatial distribution of Xiadian fault by shallow seismic reflection method. Acta Seismologica Sinica **40**(4): 399–410 (in Chinese with English abstract).

Ran YK, Chen WS, Xu XW, Chen LC, Wang H, and Li YB (2014). Late Quaternary paleoseismic behavior and rupture segmentation of the Yingxiu-Beichuan fault along the Longmen Shan fault zone, China. Tectonics **33**(11): 2 218–2 232.

Saberi E, Yassaghi A, and Djamour Y (2017). Application of geodetic leveling data on recent fault activity in Central Alborz, Iran. Geophys J Int **211**: 751–765.

Shen HY (2012). High-density Electric Prospecting Methods and Techniques. Beijing, Geological Publishing House..

Suski B, Brocard G, Authemayou C, Muralles BC, Teyssier C, and Holliger K (2010). Localization and characterization of an active fault in an urbanized area in central Guatemala by means of geoelectrical imaging. Tectonophysics **480**(1-4): 88–98.

Wang HL (1998). Active fault exploration and seismic zoning--Taking Weihai as an example..

Wang KL, Chen QF, Sun SH, and Wang AD (2006). Predicting the 1975 Haicheng Earthquake. Bull Seismol Soc Amer **96**(3): 757–795.

Wang ZC, and Chao HT (1999). The seismogenic structure of the 1995 Cangshan M_S5.2 earthquake, Shandong. Seismol Geol **21**(2): 115–120 (in Chinese with English abstract).

Wang ZC, Deng QD, Chao HT, Du XS, Shi RH, Sun ZM, Xiao LX, Min W, and Ling H (2006). Shallow-depth sonic reflection profiling studies on the active Penglai-Weihai fault zone offshore of the northern Shandong peninsula. Chin J Geophys **49**(4): 1092–1101 (in Chinese with English abstract).

Wang ZH, Cai XM, Yan JY, Wang JM, Liu Y, and Zhang L (2018). Using the integrated geophysical methods detecting active faults: A case study in Beijing, China. J Appl Geophys **156**: 82–91.

Wessel P, Smith WHF, Scharroo R, Luis J, and Wobbe F (2013). Generic mapping tools: Improved version released. EosTrans AGU **94**(45): 409–410.

Xiang HF, Han ZJ, Zhang WX, Zeng JH, and Xiao HP (2008). A preliminary study on seismologic evidence for moderate earthquake in East China. Seismol Geol **30**(1): 202–208 (in Chinese with English abstract).

Xu XW, Guo TT, Liu SZ, Yu GH, Chen GH, and Wu XY (2016). Discussion on issues associated with setback distance from active fault. Seismol Geol **38**(3): 477–502.

Xu XW, Wen XZ, Yu GH, Chen GH, Klinger Y, Hubbard J, and Shaw J (2009). Coseismic reverse- and oblique-slip surface faulting generated by the 2008 M_W7.9 Wenchuan earthquake, China. Geology **37**(6): 515–518.

Xu XW, Yeats RS, and Yu G (2010). Five short historical earthquake surface ruptures near the Silk Road, Gansu Province, China. Bull

Seismol Soc Amer **100**(2): 541–561.

Yuan DY, Wang LM, He WG, Liu BC, Ge WP, Liu XW, Liang MJ, and Zheng WJ (2008). New progress of seismic active fault prospecting in Lanzhou city. Seismol Geol **30**: 236–249 (in Chinese with English abstract).

Zheng JC, Li DM, Li CQ, Wang P, and Xu CP (2017). Rushan earthquake swarm in eastern China and its indications of fluid-triggered rupture. Earthq Sci **30**(5-6): 239–250.

Zhu JF, Huang ZL, Xu XW, Zheng RZ, Fang SM, Bai DH, Wang GC, Min W, Wen XZ, and Han ZJ (2005). Active fault exploration and seismic hazard assessment in Fuzhou city. Earthquake Research in China **19**(3): 224–239.

Zhu T, Feng R, Hao JQ, Zhou JG, Wang HL, and Wang SQ (2009). The application of electrical resistivity tomography to detecting a buried fault: A case study. J Environ Eng Geophys **14**(3): 145–151.

Zhu T, Zhou JG, and Wang HL (2017). Localization and characterization of the Zhangdian-Renhe fault zone in Zibo city, Shandong province, China, using electrical resistivity tomography (ERT). J Appl Geophys **136**: 343–352.